

Designer Fibers From 2D to 3D - Simultaneous and Controlled Engineering of Morphology, Shape and Size

Zhi-Cheng Yao ^{a,b}, Chunchen Zhang ^{a,b}, Zeeshan Ahmad ^c, Jie Huang ^d, Jing-Song Li ^a, Ming-Wei Chang ^{a,b,*}

^a Key Laboratory for Biomedical Engineering of Education Ministry of China, Zhejiang University, Hangzhou, 310027, PR China.

^b Zhejiang Provincial Key Laboratory of Cardio-Cerebral Vascular Detection Technology and Medicinal Effectiveness Appraisal, Zhejiang University, Hangzhou, 310027, PR China.

^c Leicester School of Pharmacy, De Montfort, University, The Gateway, Leicester, LE1 9BH, UK.

^d Department of Mechanical Engineering, University College London, London, WC1E 7JE, UK.

Abstract

Topography and surface morphology of micrometer and nanometer scaled fibrous biomaterials are crucial for bioactive component encapsulation, release, promoting cell proliferation and interaction within biological environment. Specifically, for drug delivery and tissue repair applications, surface engineering provides control on both aspects in tandem. In this study, the bioactive component (*ganoderma lucidum* spore polysaccharide (GLSP)) was loaded into zein prolamine (ZP) fiber matrices via coaxial electrospinning (CES) technique. During the CES process, various outer layer enveloping fluids were used to modulate fiber topography *in-situ* (from 2D to 3D). SEM and water contact angle tests indicate enveloping media impact electrospun fiber diameter (ranging from 400 nm to 3.0 μ m) and morphologies (from flat ribbon-like to solid cylindrical structures), with the latter impacting GLSP release profile. Furthermore, CCK-8 assay assessment indicates fibroblast cell proliferation (L929 cell line), while cell extension was also observed for modified ZP fibers. The results demonstrate potential applications of modified fiber morphologies, which are tailored *in-situ* without impacting chemical stability and encapsulation.

Key words: fiber morphology; zein prolamine; coaxial electrospinning; ganoderma lucidum spore polysaccharide; biocompatibility.

1. Introduction

The electrospinning (ES) technique is a one-step preparation method for engineering polymeric fibers on nanometer and micrometer scales; with extensive recent explorations in filtration, encapsulation, scaffold and biomedical remits [1-3]. Non-woven mats fabricated *via* the ES process provide numerous advantages conferred by high surface area, moisture permeability and random fiber arrangement [4, 5]. Compared to conventional single-needle ES processes, coaxial electrospinning (CES) has emerged as a valuable process to manipulate core-sheath microstructures with two or more co-flowing phases using coaxial needle devices, specifically for encapsulation applications [6].

CES effectively expands the capability of ES by enabling core-sheath nanostructures through tailoring properties and functional performances of nanomaterials [7]. More recently, the CES process has been modified; making use of solvent as the shell fluid to facilitate the process and ultimately generating high quality monolithic nano-scaled products [8]. The concept of exploiting shell solvent to modify dynamic working interfaces during ES has led to the development of tri-axial and multi-fluid complex processes [9, 10], indicating numerous possibilities for material design and development *via* solvent layering during CES. However, simultaneous and controlled engineering of fiber morphology (especially from 2D to 3D), shape and size remain limited but form important aspects in emerging micron environment analysis.

Ganoderma lucidum (GL), an edible white rot fungus, was first indexed in the *Shen Nong's Materia Medica* (206BC-8AD), and has been exploited in traditional Chinese medicine (TCM) for more than two millennia [11, 12]. The benefits of GL have been reported in several fields, including potential therapies for hepatitis, chronic bronchitis, gastritis, tumors, and immunological disorders [13, 14]. The main bioactive

components within GL are polysaccharides and triterpenoids, which are extracted from fruit bodies, mycelia and spores [15]. Despite the aforementioned properties of GL, *ganoderma lucidum* spores polysaccharide (GLSP) have been identified for antidiabetic and tissue repair benefits, especially for the treatment of chronic cutaneous wounds caused by diabetes mellitus and vascular indications (e.g. such as diabetic foot ulcers), which carry the risk of limb amputation [16, 17]. *In-vivo* experiments of GLSP present no toxicity, implying good biocompatibility, while in practice, β -D-glucan (one form of polysaccharide isolated from GLSP) is highly sensitive to oxidative degradation, including the reactions of active oxygen substances, such as hydroxyl radicals [18]. Oxidation during the storage process limits GLSP efficacy, which impedes its potential use in the pharmaceutical field [19, 20]. Thus, it is crucial to protect extracted GLSP to preserve its bio-function.

Zein prolamine (ZP), a major protein (with varying molecular weight) extracted from corn maize, is a natural polymer with several biological functions [21]. Apart from its biodegradability and biocompatibility, ZP possesses low hydrophilicity, high thermal resistance, and perfect membrane forming behavior which eludes to its potential use in biological and biomedical applications, such as coating materials in the food industry [22], carriers for drug compounds [23] and bio-scaffold components in regenerative medicine [24]. In addition, ZP has also been used as a matrix polymer to encapsulate bioactive compounds such as essential oils, colorants and antioxidants *via* both single-needle and coaxial ES [25, 26]. However, the protein is difficult to process during single-needle ES, due to high viscosities of ZP solutions. Typically, interactions between ZP and the spinneret nozzles orifice result in semi-solid blockage [27]. Previous research has, however, reported that by deploying additional solvents or non-spinnable organic sheath solvents intermittent clogging can be overcome and a

continuous ES process is achievable [23, 28]. Nevertheless, additive components may impact bio-interactions such as cell attachment and active molecule release.

In this study, the loading of GLSP into electrospun zein matrices is shown for the development of bioactive membranes with a view for skin applications. Nozzle blockage was regulating without additive inclusion (in process formulations) and a transition from ribbon to cylindrical fibers is demonstrated by deploying ethanol based formulations as enveloping fluids during the coaxial ES process. Based on the 2D-3D zein fiber type, controlled release of GLSP is shown and furthermore matrices show improved biocompatibility. While there is much data on modulating fiber surface properties we are showing controlled transition from 2D-3D aspects, which are more suited to interact with cells. These also improve cellular interaction since there is greater scope for interaction in more dimensions with greater depth. The development of such structures, and a method which enables such transitions, is crucial and timely based on advances in 3D micron-environments and the manuscript demonstrates a method for controlled engineering. This has been clarified in the manuscript

2. Materials and methods

2.1. Chemicals and materials

Zein prolamine (ZP) (Z 3625) was purchased from Sigma Aldrich (St. Louis, Mo., USA). Ethanol and phosphate buffer saline (PBS, pH=7.4) were obtained from Sinopharm Chemical Reagent Co., Ltd (Shanghai, China). High purity-grade wood-log cultivated GLS were obtained from TianHe Agricultural Group (Longquan, Zhejiang, China). A Millipore Milli-Q Reference ultra-pure water purifier (USA) was used to prepare deionized water (DI water) for operation. All chemicals were analytical grade, and used without further purification.

2.2. *Extraction of GLSP from Ganoderma Lucidum spores*

GLS was added to water to achieve a 5 w/v % mixture which was subsequently mixed using an ultrasonic device (KS-300 EI, Keshen Co., Ltd, Zhejiang, China) for 50 min at 70 °C (ultrasound irradiation, $\nu=40$ kHz), followed by centrifugation for 15 min at 12000 rpm. The supernatant was removed and stored. The above steps were repeated three times. All stored supernatant was placed into a flask, and then rotary distilled at 50 °C for 6 h. The resulting sample was freeze dried to fabricate solid polysaccharide.

2.3. *Fabrication of electrospun fibers*

ZP powder was dissolved into aqueous ethanol (80 v/v%) to prepare 45 w/v% ZP solution. During the dissolution process, a magnetic stirrer (VELP ARE heating magnetic stirrer, Italy) was used to ensure complete dissolution of ZP powder, the solution was mechanically stirred at 300 rpm under ambient temperature (25°C) for 1 h. Ethanol was mixed with DI water to achieve different concentrations (20, 40, 60, 80 v/v%), and used as the outer enveloping liquid during the CES process.

In order to investigate the impact of enveloping liquids physical properties on fiber morphology; the viscosity and electrical conductivity of all enveloping media were measured. 2 mL of each liquid sample was added into the pre-defined stainless steel wells of the viscometer (LVDV-II, Brookfield, USA), and then, viscosity was obtained at 25 °C using a S21 spindle at 140 rpm. Electrical conductivity was measured using a YSI 3200 electrical conductivity meter (YSI, USA) at 25 °C. All measurements were operated in triplicate and mean values were obtained.

Modified ZP fibers were fabricated using a CES apparatus, as shown in **Fig. 1a**. The device includes a high power voltage supply (Glassman high voltage Inc. series FC,

USA), two precision syringe pumps (KD Scientific KDS100, USA), a coaxial stainless steel needle and a collector connected to the grounded electrode. The CES system comprises two enveloped needles. The inner and outer diameters of the inner needle are 0.2 and 0.4 mm, while the outer needle possesses dimensions of 0.9 and 1.2 mm, respectively. Individual ZP solution was loaded into 5 mL plastic syringe, and propelled from the syringe via silicon tubing into the inner inlet of the coaxial device (flow rate: 0.8-1.2 mL/h). Ethanol solutions with different concentrations (enveloping liquids) were individually loaded into a separate syringe and perfused into the outer needle of the coaxial system at a flow rate of 1.0 mL/h. An electric field (14-16 kV) was applied between the coaxial needle and grounded electrode. Aluminum foil was used as the fiber collector substrate, contacted with grounded electrode, and placed directly below the needle exit at a distance of 15 cm. The ES jetting modes were observed using a high-speed camera (Baumner TXG03C, Germany). All experiments were performed at the ambient temperature (25 °C). Different conditions are listed in **Tab. 1** for fabricating ZP fibers.

2.4. Fiber morphology, and water contact angle measurements

Scanning electron microscopy (SEM, FEI Quanta 650, Utrecht, Netherlands) was used to assess morphology, diameter and size distribution of fabricated fibers. SEM images were obtained at an accelerating voltage of 20 kV. All samples were assessed on metallic stubs by double-backed conductive tape, and sputter-coated with a thin layer of gold using a desktop sputter coater (108 Auto coater, Cressington Scientific Instruments, Herts, UK) for 60 s at a current intensity of 25 mA to prevent sample charging. The micrographs were assessed using ImageJ software (National Institute of Health, MD, USA) to measure fiber diameter. Aspect ratio (AR) was used to determine

the cross section of ZP fibers (and their shape) by measuring the minor and major axes, and was calculated using Eq. (1):

$$\text{Aspect ratio (\%)} = \frac{\text{Minor axis of the fiber cross section}}{\text{Major axis of the fiber cross section}} \times 100\% \quad (1)$$

For each sample, 100 random fibers were assessed. All data as exported for analysis, and statistical graphs were plotted using Origin software (OriginLab, USA).

In order to investigate hydrophobicity/hydrophilicity of ES fibrous membranes, water contact angle (WCA) measurements were obtained with an optical contact angle meter (SL200KB, KINO Industry Co. Ltd., USA). Fibrous non-woven samples with thickness of ~0.1 mm were collected and subsequently layered onto an object slide. The measurements were performed using a 3-axis horizontal tilt stage and observed in the sessile drop mode at 25 °C. A water droplet (~10 µL) was pipetted on to each membrane sample. The mean value of left and right WCAs on each sample was recorded 2 s after droplet release, when the droplet status acclimatized. The mean of three measurement readings was obtained.

2.5. FTIR spectroscopy

Chemical interactions and material stability of ES fibers were assessed using a Fourier transform infrared (FTIR) spectrometer (IR Affinity 1, Shimadzu, Japan). 2 mg of each sample was mixed with 200 mg KBr powder by grinding in a mortar. The mixture was then pressed into a transparent pellet under a pressure of ~20 MPa. Each spectrum was acquired from 20 scans. A scanning range of 4000-400 cm⁻¹ was used, when the resolution was 4 cm⁻¹.

2.6. GLSP loading and in-vitro release

ZP composite membranes were washed using PBS for 30 s to obtain the quantity of un-encapsulated GLSP, which was mainly distributed on the surface of the membrane. Loading capacity (LC) of GLSP presents the quantity of GLSP encapsulated within ZP matrix, and was determined using Eq. (2) [29, 30]:

$$LC (\%) = \frac{\text{Amount of GLSP content entrapped in fibrous membranes (mg)}}{\text{Weight of fibrous membranes (mg)}} \times 100\% \quad (2)$$

The un-encapsulated GLSP was dissolved in PBS. Thus, the encapsulation efficiency (EE) of GLSP within ZP membranes was determined using Eq. (3) [29, 30]:

EE

$$(\%) = \frac{\text{Amount of GLSP content entrapped in fibrous membranes (mg)}}{\text{Theoretical total amount of GLSP (mg)}} \times 100\% \quad (3)$$

The quantity of GLSP entrapped in ZP was determined by calculating the difference between the total quantity of GLSP added into the ZP matrix and the amount of washed-GLSP. The GLSP content in PBS solution was determined by measuring absorbance at 221 nm (the characteristic UV-Vis absorption of GLSP) in triplicate using a UV-2600 spectrophotometer (Shimadzu, Japan).

For *in-vitro* release, approximately 50 mg of individual ZP/GLSP composite fiber membranes (engineering formulation: single-needle ES ZP fiber; coaxial ES ZP-40, 60, and 80 fibers) were placed into 10 mL PBS and incubated at 37 °C. At designed time intervals, 2 mL of supernatant was removed from the assessment medium and replaced with 2 mL of fresh test medium. The supernatant was filtered (0.45 μm Millipore), and assessed using UV-Vis analysis. The percentage of GLSP released was calculated using Eq. (4) [18]:

$$GLSP \text{ release } (\%) = \frac{Q_t}{Q_s} \times 100\% \quad (4)$$

Here, Q_t is the quantity of GLSP released at time t , Q_s is the total quantity released.

2.7. *In-vitro biological evaluation*

To investigate the effect of fibrous morphology and GLSP loading on ZP composite membrane biocompatibility (single-needle ES ZP fibers, single-needle ES ZP/GLSP composite fibers, and coaxial ES ZP-80/GLSP composite fibers), fibroblast cells (L929 cell lines) were used to assess cytotoxicity. L929 cells were incubated and maintained in MEM medium supplied with 10% FBS at 37 °C, in 5% CO₂. The culture medium was changed every 2 d. ES fibrous non-woven was collected for 1 h, and cut into discs (diameter=6 mm). Fibrous discs were sterilized under UV light for 2 h, and were then added to cell culture plates. 100 μL L929 cell suspension was transferred to a 96-well plate at a density of 1.5×10⁴ cells/well and incubated for 24 h.

At 6, 12 and 24 h during cell culture, a Cell Counting Kit-8 (CCK-8) assay was set to evaluate proliferation of L929 cells. By adding 20 μL CCK-8 solution to each well and incubating for further 3 h, absorbance was measured at a wavelength of 450 nm using a microplate reader (Multiskan GO, Thermo Fisher Scientific, USA). Cell viability in polystyrene well plate was used as a control and the culture medium with CCK-8 solution was utilized as a blank. The relative cell viability was calculated as Eq. (5) [31]:

$$\text{Cell viability (\%)} = \frac{\text{Ab. (sample)} - \text{Ab. (blank)}}{\text{Ab. (control)} - \text{Ab. (blank)}} \times 100\% \quad (5)$$

Where Ab. means the absorbance.

In addition, for cell morphology assessment, L929 cells were seeded on 3 types of fibrous ZP membranes (single-needle ES ZP fibers, single-needle ES ZP/GLSP composite fibers, and CES ZP-80/GLSP composite fibers) at a density of 5×10⁵ cells/mL. After 24 h incubation, cells were fixed using 4 v/v% formalin for 15 min at

ambient temperature, and then washed using PBS. Cells were then permeabilized using 0.1 % Triton X-100 for 10 min. The cell cytoskeleton and nuclei were stained with Alexar Fluor 546 phalloidin (Invitrogen, Carlsbad, California, USA) (1:100 dilution) and 4', 6'-diamidino-2-phenylindole hydrochloride (DAPI, Invitrogen) for 1 min and 5 min, respectively. Samples were then washed with PBS, and visualized using an inverted fluorescence microscope (Nikon Ti-S, Japan). The experimental timescale (24 h) was according to previous studies[32, 33], while staining procedure and dye inclusion were also followed based on previous studies[34, 35].

2.8. *Statistical analysis*

All experiments were performed in triplicate and data is presented as mean \pm standard deviation (n=3). Statistical analysis was performed using SPSS software (SPSS Statistics v 18, IBM, UK), and statistically significant differences between variables were assessed via one-way analysis of variance (ANOVA) followed by student's t-Test (*P<0.05).

3. Results and discussion

3.1. Fabrication of ZP fibers and fibrous membranes

Experimental conditions during assessment of variable parameters were kept constant. These include the ambient (laboratory) temperature, humidity and the deposition distance.

The cone-jet mode is crucial to achieve near-uniform fibrous structures during the ES process [36]. As shown in **Fig. 1b-III**, during single-needle ES process, three seconds post processing, a semi-solid substance was formed which resulted in spinneret blockage. Fiber fabrication is achievable but this requires manual removal of solidified polymer at the nozzle exit. During the ES operation, an uneven distribution of charge carried by jets arises due to solvent evaporation and jet-elongation. A reduction in jet local surface charge density is often observed due to ejection of smaller jets from the surface of the primary jet or through jet-splitting [37]. Further evaporation of the solvent yields semi-solid polymer agglomeration which ultimately impedes the spinning process. In contrast to single-needle ES, using ethanol as the enveloping liquid via CES operation (outer fluid: 80 or 100 w/v% ethanol) can improve this limitation, and achieve stable fiber preparation. Without changing ZP formulation constituents for the CES process, a series of ethanol based enveloping liquids (a variation of ethanol solutions) were deployed. **Fig. 1c** presents the dripping, transition, and continuous spinning modes during the CES process (outer fluid: 80 w/v% ethanol). As shown in **Fig. 1c-III**, a linear fluid jet was emitted from the spinneret. Due to ZP solubility in ethanol and considering the loading concentration range (70 to 92 v/v%) [38], the co-flowing system inhibits clog formation and a stable continuous spinning mode is achieved. However, when the

concentration of ethanol solution is too low (20, 40, and 60 w/v% in this study), blockage is not improved.

Fig. 2 presents SEM images of ZP fibers collected at different conditions. Original ZP fibers obtained via single-needle ES process are shown in **Fig. 2a**. The fibers present flat ribbon-like structures, while upon addition of ethanol solutions as outer enveloping layer during co-flow; cylindrical structures are obtained (shown in **Figs. 2b-f**). The fiber size distribution is influenced by the enveloping medium. As the inserts show in **Figs. 2a-f**, the mean single-needle ZP fiber diameter was $1.65\pm 0.38\ \mu\text{m}$, and fibers from structures engineered using outer 20, 40, 60, 80 and 100 v/v% ethanol solutions were 1.72 ± 0.51 , 1.18 ± 0.43 , 0.99 ± 0.35 , 0.49 ± 0.09 and $0.49\pm 0.11\ \mu\text{m}$, respectively.

As shown in **Fig. 2g**, by gauging the major and minor axes of resulting fibers, ARs of all six engineered fiber systems was obtained, which indicates the impact of ethanol solution concentration. AR of single-needle ZP fiber is $34.5\pm 9.3\%$, indicating a flat structure across its cross section. ARs of fibers fabricated *via* CES process are 49.7 ± 11.1 , 48.0 ± 9.1 , 50.1 ± 10.1 , 63.6 ± 10.6 and $64.7\pm 9.9\%$, when the enveloping ethanol solution concentrations were 20, 40, 60, 80 and 100 v/v%, respectively. The results shows an increase in fiber AR with volume of ethanol in the enveloping medium, During the CES process, the outer fluid prevents rapid evaporation of the core solvent, inhibiting premature evaporation of the vehicle from the core polymeric matrix system. Thus, the subsequent retention of a liquid jet, as opposed to a solidifying form, enables it to remain within the instability region for a longer time period before complete solidification [39], which can be used to regulates fiber surface.

Variations arising in fiber AR and diameter are mainly due to physical properties of the spinning fluids; where the surface tension and electrical conductivity of the core

solution are mainly responsible for enabling Taylor cone formation during the ES process [40]. During single-needle ES, the physical properties of ZP solutions dominate the process. While in the modified CES process, properties of the enveloping solutions (conductivity and surface tension) crucially contribute towards and influence Taylor cone aspects, and therefore impact resulting fiber size distribution. This is also dependent on the viscosity of spinning liquids [41, 42]. As shown in **Fig. 3**, solution viscosity varies depending on the ratio of water to ethanol. In this study, 40 and 60 v/v% ethanol solutions present larger viscosities compared to other concentrations, which is mainly due to the molecule interaction at the comparative amounts [21]. During the ES process, attractive forces between the two electrodes (nozzle and ground), the repulsion forces between the two unstable bending coils and Coulombic repulsion within the fluid jet synergistically influence the electric field force and travelling distance of ejected liquid, and further modulate fiber formation [41]. The reduced electrical conductivity with increasing ethanol concentration elongates the travelling distance of ES fibers between the two electrodes (nozzle and ground), which in turn leads to a decrease in fiber diameter.

3.2. Surface hydrophobicity

Hydrophilicity/hydrophobicity of fabricated fibrous membranes, which is mainly determined by its surface chemical composition and surface topography, is critical for biological applications, such as drug release, cell adhesion and proliferation at the biological interface [24]. Conventionally, the degree of WCA is classified into several categories according to the angle value. For a surface with WCA in the range of 25-90°, the membrane is defined to be highly hydrophilic, while for a surface with WCA in the range of 90-150°, the material is considered to be hydrophobic. If the WCA is lower

than 25° , or greater than 150° , the material is considered superhydrophilic or superhydrophobic, respectively [37]. WCAs of prepared ES fibrous membranes are shown in **Fig. 4**. Mean WCA of membrane obtained via single-needle ES is $88.1 \pm 2.1^\circ$, while the WCAs of modified membranes fabricated with CES operation (ZP-20, 40, 60, 80 and 100) are 78.3 ± 4.6 , 105.6 ± 2.4 , 112.1 ± 4.5 , 122.9 ± 2.3 , and $132.3 \pm 1.6^\circ$, respectively, indicating magnified hydrophobicity with increasing enveloping ethanol concentration. Variation to membrane surface hydrophobicity is mainly due to differences in diameter size distribution and surface topography of ES fibers [43]. As shown in **Figs. 2a-f**, compared to modified ZP fibers prepared using 80 and 100 w/v% ethanol solution as outer fluids during CES process, fibers prepared via single-needle ES using ethanol solutions with low concentrations (20, 40, and 60 w/v%) present flat ribbon-like morphology, which limits the quantity of trapped air at the fiber membrane-water interface, and further results in reduced WCAs.

3.3. Effect of process parameters on fiber diameters

Several scaling and operational laws govern the CES process, such as the solution and process parameters [44]. Additionally, during the CES operation, solutions with greater electrical conductivity drive the ES process and in this instance the core ZP solutions are responsible for this feature [45]. The driving liquid in CES process dominates the co-flow behavior. Hence, the effect of flow rate on fiber diameter was investigated during the ES and CES process by varying the driving liquid feed rate from 0.8 to 1.2 mL/h. **Fig. 5a** highlights the relationship between the flow rate and ZP mean fiber diameter. An increase in mean fiber diameter with increasing solution flow rate can be observed in both single-needle ES and CES formats. At a feed rate of 0.8 mL, the mean fiber diameter is $1.53 \pm 0.5 \mu\text{m}$ for single-needle ES, while mean fiber diameter for

samples prepared via CES (using 80 w/v% ethanol as outer fluid) is $0.41\pm 0.17\ \mu\text{m}$. When feed rate is increased to 1.2 mL/h, mean fiber diameters of single-needle ES and CES fibers are 2.00 ± 0.40 and $0.80\pm 0.12\ \mu\text{m}$, respectively. This is caused by the increasing amount of solution and therefore polymeric medium contributing towards fibers.

The effect of applied voltage on fiber size distribution was investigated by manipulating the electric field over a pre-determined range (14-16 kV). Reduction in mean ZP fiber diameter are found for both single-needle ES and CES processes, when increasing the voltage from 14 to 16 kV. At 14 kV, mean fiber diameter obtained via single-needle ES is $3.00\pm 0.68\ \mu\text{m}$, while for those prepared via CES using 80 w/v% ethanol as sheath liquid is $1.70\pm 0.35\ \mu\text{m}$. A reduction in mean fiber diameter to 1.21 ± 0.42 and $0.43\pm 0.21\ \mu\text{m}$, respectively, following an increase to the applied voltage (to 16 kV) is observed. Increasing the applied voltage facilitates electrostatic repulsive force on the jet, which ultimately causes a reduction in the mean fiber diameter [46].

3.4. Composition and release profile from ZP matrix

GLSP was encapsulated into ZP matrices prepared via single-needle ES and CES using 40, 60, and 80 w/v% ethanol solution as outer enveloping liquids. FTIR spectroscopy was used to examine the chemical structures and material stability of ZP fiber matrix and encapsulated GLSP. **Fig. 6** shows the infrared spectra of pure ZP powder, GLSP, and ES fiber composites (ZP-40, 60, and 80). The broad peak at $1650\ \text{cm}^{-1}$ corresponds to the α helical structure [47], and peak at $1515\ \text{cm}^{-1}$ indicates the amide II band [48]. Components of GLSP are also detected at 1035 and $1079\ \text{cm}^{-1}$, corresponding to C-N stretching of amine groups within polysaccharide [20]. By comparing the FTIR spectra

in **Fig. 6**, there is no obvious variation of characteristic peaks of ZP and GLSP, indicating the efficient encapsulation of GLSP into ZP fibrous matrix via CES process. The ES process is an efficient route to load bioactive components into micro/nanoparticles or fibers in a single step [42, 49]. Evaluating encapsulation effect and loading capacity (LC) provides an indication on GLSP encapsulation feasibility into ZP fibrous matrix per unit weight, while encapsulation efficiency (EE) indicates the remaining GLSP within the fibrous structure post ES process. **Fig. 7a** shows LC and EE of GLSP within the ZP matrix. It can be found that, compared to the LC of GLSP via single-needle ES process, which is $14.5\pm 0.2\%$, there is no noticeable difference between processes. The LCs of GLSP are 14.9 ± 0.1 , 15.0 ± 0.1 and $15.9\pm 0.1\%$ for ZP-40, 60 and 80 samples, respectively. The EE values of GLSP within the matrix fabricated using ZP-40, 60, and 80 are 81.7 ± 0.6 , 82.3 ± 0.5 , and $87.2\pm 0.7\%$, respectively, which also show no significant differences when compared to the EE value of single-needle ES process ($79.7\pm 1.0\%$). These results suggest the CES process, as used for fiber modulation, does not impede drug loading or encapsulation efficiency into electrospun matrices.

Fig. 7b shows the cumulative release percentage of GLSP during 10 h incubation period. GLSP exhibits an initial burst release in the first 2 h for all the four sample groups, which is a common phenomenon for active-loaded fibers resulting from drug accumulation on fiber surface and inherent high surface areas [50]. The percentage release of GLSP in ZP, ZP-40 and ZP-80 increases to 87.6 ± 3.9 , 84.4 ± 4.0 and $82.4\pm 3.7\%$ at 4 h, while the value of the ZP-60 fiber is $66.2\pm 3.3\%$. Drug release from matrix type systems is usually a diffusion process. Compared to flat ribbon-like structures, cylindrical fibers exhibit a more sustained-release profile [39, 51]. SEM images shown in **Fig. 2**, show ZP-80 fibers to exhibit cylindrical morphologies, while ZP, ZP-40 and

ZP-60 fibers present flat topographies. As presented in **Figs. 2d&e**, ZP-80 mean fiber diameter is $0.49\pm 0.09\ \mu\text{m}$, which is nearly half that of ZP-60 samples ($0.99\pm 0.35\ \mu\text{m}$). Fibers with larger mean diameter release drug at much slower rates [52].

In order to propose a GLSP release mechanism from fibrous membranes, Higuchi, Hixson-Crowell, and Korsmeyer-Peppas models were applied to evaluate in vitro release kinetics. In the Higuchi model, the linear relationship between cumulative release quantity and the square root of time indicates the likelihood of a diffusion-controlled underlying mechanism.

The Higuchi model is expressed as shown in Eq. (6)

$$M_t = k_H t^{1/2} \quad (6)$$

Where M_t is the cumulative quantity of drug released at time t , and k_H is the Higuchi constant [53].

The Hixson-Crowell model gives as Eq. (7)

$$M_t = M_\infty (1 - (1 - \alpha t)^3) \quad (7)$$

Where M_∞ is the total quantity of GLSP released from the fibrous membranes, M_t is the fraction of GLSP released in time t , and $\alpha = 9k_{HC}/r_0$, which depends on the release constant of Hixson-Crowell model (k_{HC}) and the initial radius r_0 [54].

The Korsmeyer-Peppas model is expressed as shown in Eq. (8):

$$M_t/M_\infty = kt^n \quad (8)$$

Here, M_t and M_∞ indicate the percentage of drug released at time t and infinite time ∞ , respectively. The k value is a characteristic constant, when n is the release exponent. A release exponent value below 0.45 indicates Fickian diffusion or case-I diffusion, while an n value, greater than 0.85, indicates case-II diffusion, which implies certain interactions existing among drug molecules, release medium and the delivery matrix.

When n value is in the range of 0.45 to 0.85, an anomalous transport process is proposed,

which involves multiple factors contributing towards the release mechanism.

Based on R^2 values, the best fitting model was the Higuchi function. The corresponding fitting results are presented in **Tab. 2**, which strongly suggest GLSP release from ZP matrices follows a diffusive release mechanism. For the Korsmeyer-Peppas model fitting shown in **Tab. 2**, n values for the present study are 0.26, 0.20, 0.26 and 0.26 for each composite sample. The results demonstrate GLSP release from all composite fibers is *via* typical Fickian diffusion mechanism (all exponents < 0.45), indicating the deployment of enveloping ethanol during CES operation has limited influence on GLSP release mechanism. Variations to k values suggest fibers could be engineered to tailor drug release as confirmed in **Fig.7b**.

3.5. *Biological evaluation of electrospun fibrous membranes*

In this study, bioactive membranes were assessed for cell viability analysis over a 24-hour period, which is typically used for wound dressing/healing material applications. Therefore, experimental protocol was based on this timescale [32, 33]. In addition, staining procedure and dye inclusion were also followed based on previous studies [34, 35].

Cell viability indicates membrane biocompatibility, and is determined by contrasting test groups (ES fibers) with the control. Herein, L929 cells were cultured for 24 h, and a CCK-8 assay was performed to examine the impact of various electrospun structures on L929 cell proliferation. Membranes were prepared from single-needle ZP, single-needle ZP/GLSP and CES ZP-80/GLSP. As shown in **Fig. 8a**, cell proliferation on pure ZP fibrous membrane exhibits no significant difference to the control group at post 6 and 12 h incubation time, indicating negligible cytotoxicity. Furthermore, continuously increasing cells numbers in ZP/GLSP and ZP-80/GLSP groups indicate membranes are

non-toxic and support cell proliferation. Compared to pure ZP membranes, cell proliferation in groups comprising GLSP is noted to be significantly high, especially at post 24 h incubation time, indicating GLSP promotes proliferation of fibroblast cells. Morphology of proliferated L929 cells was confirmed using fluorescent microscopy once cells were stained red for F-actin and blue for cell nuclei. As shown in **Fig. 8b**, in contrast to cell behavior on pure ZP membranes, ZP/GLSP membranes promote cell attachment, while ZP-80/GLSP membranes show profound cell growth and extension on the membrane. The result indicate GLSP improves cell affinity towards embedded electrospun fibers. Additionally, when compared to flat ribbon-like structures prepared *via* single-needle ES; cylindrical morphologies fabricated using CES process also facilitate cell growth on the membrane surface.

4. Conclusion

In summary, ZP fibers with diameters ranging from 400 nm to 1.7 μm were prepared via a modified CES process incorporated various ethanol solutions as enveloping liquids. Various topographies and surface hydrophobicity were achieved by careful selection of specific ethanol solutions. FTIR analysis indicated successful and stable encapsulation of GLSP within ZP fibrous mats. LC and EE of GLSP were 15% and 85%, respectively, in all the single-needle ES and modified CES process groups. Distinctive release profile was observed in the ZP-60 group due to the influence of fiber size distribution and aspect ratio. CCK-8 assay conducted on L929 cell lines demonstrates good cytocompatibility for all test samples (ZP, ZP/GLSP, and ZP-80/GLSP), and GLSP role in cell proliferation was observed. Fluorescent images confirm encapsulated GLSP supports extension and proliferation of fibroblast cells (L929 cell line), which indicates potential application in drug delivery and tissue repair.

Acknowledgements

This work was financially supported by the National Nature Science Foundation of China (No. 81771960), the Fundamental Research Funds for the Central Universities (2017QNA5017) and Key Technologies R&D Program of Zhejiang Province (2015C02035).

References

- [1] B. Sun, Y.Z. Long, H.D. Zhang, M.M. Li, J.L. Duvaill, X.Y. Jiang, H.L. Yin, Advances in three-dimensional nanofibrous macrostructures via electrospinning, *Prog. Polym. Sci.* 39 (2014) 862-890.
- [2] L. Wang, M.W. Chang, Z. Ahmad, H. Zheng, J.S. Li, Mass and controlled fabrication of aligned PVP fibers for matrix type antibiotic drug delivery systems, *Chem. Eng. J.* 307 (2016) 661-669.
- [3] J.C. Wang, H. Zheng, M.W. Chang, Z. Ahmad, J.S. Li, Preparation of active 3D film patches via aligned fiber electrohydrodynamic (EHD) printing, *Sci. Rep.* 7 (2017) 43924.
- [4] S. Koushkbaghi, P. Jafari, J. Rabiei, M. Irani, M. Aliabadi, Fabrication of PET/PAN/GO/Fe₃O₄ nanofibrous membrane for the removal of Pb(II) and Cr(VI) ions, *Chem. Eng. J.* 301 (2016) 42-50.
- [5] H. Beheshti, M. Irani, L. Hosseini, A. Rahimi, M. Aliabadi, Removal of Cr (VI) from aqueous solutions using chitosan/MWCNT/Fe₃O₄ composite nanofibers-batch and column studies, *Chem. Eng. J.* 284 (2016) 557-564.
- [6] B. Wang, H. Zheng, M.W. Chang, Z. Ahmad, J.S. Li, Hollow polycaprolactone composite fibers for controlled magnetic responsive antifungal drug release, *Colloids Surf. , B* 145 (2016) 757-767.
- [7] Y. Xu, J.J. Li, D.G. Yu, G.R. Williams, J.H. Yang, X. Wang, Influence of the drug distribution in electrospun gliadin fibers on drug-release behavior, *Eur. J. Pharm. Sci.* 106 (2017) 422-430.
- [8] Q. Wang, D.G. Yu, L.L. Zhang, X.K. Liu, Y.C. Deng, M. Zhao, Electrospun hypromellose-based hydrophilic composites for rapid dissolution of poorly water-soluble drug, *Carbohydr. Polym.* 174 (2017) 617-625.
- [9] D.G. Yu, J.J. Li, M. Zhang, G.R. Williams, High-quality Janus nanofibers prepared using three-fluid electrospinning, *Chem. Commun.* 53 (2017) 4542 - 4545.
- [10] G.Z. Yang, J.J. Li, D.G. Yu, M.F. He, J.H. Yang, G.R. Williams, Nanosized sustained-release drug depots fabricated using modified tri-axial electrospinning, *Acta Biomater.* 53 (2017) 233-241.
- [11] M. Haou-Tzong, H. Jung-Feng, C. Shui-Tein, Anti-diabetic effects of *Ganoderma lucidum*, *Phytochemistry* 114 (2015) 109 - 113.
- [12] J. Zhang, X. Gao, Y. Pan, N. Xu, L. Jia, Toxicology and immunology of *Ganoderma lucidum* polysaccharides in Kunming mice and Wistar rats, *Int. J. Biol. Macromol.* 85 (2016) 302-310.
- [13] D. Pan, D. Zhang, J. Wu, C. Chen, Z. Xu, H. Yang, P. Zhou, A novel proteoglycan from *Ganoderma lucidum* fruiting bodies protects kidney function and ameliorates diabetic nephropathy via its antioxidant activity in C57BL/6 db/db mice, *Food Chem. Toxicol.* 63 (2014) 111-118.
- [14] C.W. Ma, M. Feng, X. Zhai, M. Hu, L. You, W. Luo, M. Zhao, Optimization for the extraction of polysaccharides from *Ganoderma lucidum* and their antioxidant and antiproliferative activities, *J. Taiwan Inst. Chem. Eng.* 44 (2013) 886-894.
- [15] K. Pan, Q. Jiang, G. Liu, X. Miao, D. Zhong, Optimization extraction of *Ganoderma lucidum* polysaccharides and its immunity and antioxidant activities, *Int. J. Biol. Macromol.* 55 (2013) 301-306.
- [16] X. Li, Y. Liu, J. Zhang, R. You, J. Qu, M. Li, Functionalized silk fibroin dressing with topical bioactive insulin release for accelerated chronic wound healing, *Mater. Sci. Eng. , C* 72 (2017) 394-404.
- [17] P.G. Cheng, C.W. Phan, V. Sabaratnam, N. Abdullah, M.A. Abdulla, U.R. Kuppasamy, Polysaccharides-rich extract of *ganoderma lucidum* (M.A. Curtis:Fr.) P. karst accelerates wound healing in streptozotocin-induced diabetic rats, *Evid.-based Compl. Alt.* 2013 (2013) 671252.
- [18] D. Zhao, J.S. Li, W. Suen, M.W. Chang, J. Huang, Preparation and characterization of *Ganoderma lucidum* spores-loaded alginate microspheres by electrospinning, *Mater. Sci. Eng. , C* 62 (2016) 835-

842.

- [19] R. Kivelä, U. Henniges, T. Sontag-Strohm, A. Potthast, Oxidation of oat β -glucan in aqueous solutions during processing, *Carbohydr. Polym.* 87 (2012) 589-597.
- [20] Z.C. Yao, L.J. Jin, Z. Ahmad, H. Jie, M.W. Chang, J.S. Li, Ganoderma lucidum polysaccharide loaded sodium alginate micro-particles prepared via electrospraying in controlled deposition environments, *Int. J. Pharm.* 524 (2017) 148-158.
- [21] C. Yao, X. Li, T. Song, Electrospinning and crosslinking of zein nanofiber mats, *J. Appl. Polym. Sci.* 103 (2006) 380-385.
- [22] Y.P. Neo, S. Ray, J. Jin, M. Gizdavic-Nikolaidis, M.K. Nieuwoudt, D. Liu, S.Y. Quek, Encapsulation of food grade antioxidant in natural biopolymer by electrospinning technique: a physicochemical study based on zein-gallic acid system, *Food Chem.* 136 (2013) 1013-1021.
- [23] Y.N. Jiang, H.Y. Mo, D.G. Yu, Electrospun drug-loaded core–sheath PVP/zein nanofibers for biphasic drug release, *Int. J. Pharm.* 438 (2012) 232-239.
- [24] N. Liao, M.K. Joshi, A.P. Tiwari, C.H. Park, C.S. Kim, Fabrication, characterization and biomedical application of two-nozzle electrospun polycaprolactone/zein-calcium lactate composite nonwoven mat, *J. Mech. Behav. Biomed. Mater.* 60 (2016) 312-323.
- [25] Y. Zhang, X. Liu, Y. Wang, P. Jiang, S.Y. Quek, Antibacterial activity and mechanism of cinnamon essential oil against Escherichia coli and Staphylococcus aureus, *Food Control* 59 (2016) 282-289.
- [26] A. Fernandez, S. Torres-Giner, J.M. Lagaron, Novel route to stabilization of bioactive antioxidants by encapsulation in electrospun fibers of zein prolamine, *Food Hydrocolloids* 23 (2009) 1427-1432.
- [27] K. Kanjanapongkul, S. Wongsasulak, T. Yoovidhya, Prediction of clogging time during electrospinning of zein solution: Scaling analysis and experimental verification, *Chem. Eng. Sci.* 65 (2010) 5217-5225.
- [28] D.G. Yu, J.H. Yu, L. Chen, G.R. Williams, X. Wang, Modified coaxial electrospinning for the preparation of high-quality ketoprofen-loaded cellulose acetate nanofibers, *Carbohydr. Polym.* 90 (2012) 1016-1023.
- [29] S. Chatterjee, Z.M. Judeh, Encapsulation of fish oil with N-stearoyl O-butylglyceryl chitosan using membrane and ultrasonic emulsification processes, *Carbohydr. Polym.* 123 (2015) 432-442.
- [30] K. Moomand, L.T. Lim, Oxidative stability of encapsulated fish oil in electrospun zein fibres, *Food Res. Int.* 62 (2014) 523-532.
- [31] M. He, H. Jiang, R. Wang, Y. Xie, C. Zhao, Fabrication of metronidazole loaded poly (ϵ -caprolactone)/zein core/shell nanofiber membranes via coaxial electrospinning for guided tissue regeneration, *J. Colloid Interface Sci.* 490 (2017) 270-278.
- [32] W.A. Sarhan, H.M.E. Azzazy, I.M. Elsherbiny, Honey/Chitosan Nanofiber Wound Dressing Enriched with Allium sativum and Cleome droserifolia: Enhanced Antimicrobial and Wound Healing Activity, *ACS Appl. Mater. Interfaces* 8 (2016) 6379-6390.
- [33] H. Hajiali, M. Summa, D. Russo, A. Armirotti, V. Brunetti, R. Bertorelli, A. Athanassiou, E. Mele, Alginate–lavender nanofibers with antibacterial and anti-inflammatory activity to effectively promote burn healing, *J. Mater. Chem. B* 4 (2016) 1686-1695.
- [34] D. Li, T. Wu, N. He, J. Wang, W. Chen, L. He, C. Huang, H.A. Ei-Hamshary, S.S. Al-Deyab, Q. Ke, Three-dimensional polycaprolactone scaffold via needleless electrospinning promotes cell proliferation and infiltration, *Colloids Surf., B* 121 (2014) 432-443.
- [35] B. Wang, W. Zhou, M.W. Chang, Z. Ahmad, J.S. Li, Impact of substrate geometry on electrospun fiber deposition and alignment, *J. Appl. Polym. Sci.* 134 (2017) 44823.

- [36] G. Yuan, Z. Ding, M.W. Chang, Z. Ahmad, J.S. Li, Optimising the shell thickness-to-radius ratio for the fabrication of oil-encapsulated polymeric microspheres, *Chem. Eng. J.* 284 (2016) 963-971.
- [37] X. Xu, L. Jiang, Z. Zhou, X. Wu, Y. Wang, Preparation and Properties of Electrospun Soy Protein Isolate/Polyethylene Oxide Nanofiber Membranes, *ACS Appl. Mater. Interfaces* 4 (2012) 4331-4337.
- [38] W. Li, Y. Han, H. Yang, G. Wang, R. Lan, J.Y. Wang, Preparation of microcarriers based on zein and their application in cell culture, *Mater. Sci. Eng. , C* 58 (2016) 863-869.
- [39] J.M. Yang, L.S. Zha, D.G. Yu, J. Liu, Coaxial electrospinning with acetic acid for preparing ferulic acid/zein composite fibers with improved drug release profiles, *Colloids Surf. , B* 102 (2013) 737-743.
- [40] Z.C. Yao, Y. Gao, M.W. Chang, Z. Ahmad, J.S. Li, Regulating poly-caprolactone fiber characteristics in-situ during one-step coaxial electrospinning via enveloping liquids, *Mater. Lett.* 183 (2016) 202-206.
- [41] H.F. Wen, C. Yang, D.G. Yu, X.Y. Li, D.F. Zhang, Electrospun zein nanoribbons for treatment of lead-contained wastewater, *Chem. Eng. J.* 290 (2016) 263-272.
- [42] Z.C. Yao, M.W. Chang, Z. Ahmad, J.S. Li, Encapsulation of rose hip seed oil into fibrous zein films for ambient and on demand food preservation via coaxial electrospinning, *J. Food Eng.* 191 (2016) 115-123.
- [43] Z.C. Yao, S.C. Chen, Z. Ahmad, J. Huang, M.W. Chang, J.S. Li, Essential Oil Bioactive Fibrous Membranes Prepared via Coaxial Electrospinning, *J. Food Sci.* 82 (2017) 1412-1422.
- [44] S. Agarwal, A. Greiner, J.H. Wendorff, Functional materials by electrospinning of polymers, *Prog. Polym. Sci.* 38 (2013) 963-991.
- [45] I.G. Loscertales, A. Barrero, I. Guerrero, R. Cortijo, M. Marquez, A.M. Gañán-Calvo, Micro/nano encapsulation via electrified coaxial liquid jets, *Science* 295 (2002) 1695-1698.
- [46] N. Bhardwaj, S.C. Kundu, Electrospinning: A fascinating fiber fabrication technique, *Biotechnol. Adv.* 28 (2010) 325-347.
- [47] L.A. Forato, A.C. Doriguetto, H. Fischer, Y.P. Mascarenhas, A.F. Craievich, L.A. Colnago, Conformation of the Z19 prolamin by FTIR, NMR, and SAXS, *J. Agric. Food Chem.* 52 (2004) 2382-2385.
- [48] T. Gillgren, S.A. Barker, P.S. Belton, D.M. Georget, M. Stading, Plasticization of zein: a thermomechanical, FTIR, and dielectric study, *Biomacromolecules* 10 (2009) 1135-1139.
- [49] Y.K. Song, K.H. Cha, D.G. Song, D. Chung, C.H. Pan, Microencapsulation of peppermint oil in an alginate-pectin matrix using a coaxial electro spray system, *Int. J. Food Sci. Tech.* 49 (2014) 733-739.
- [50] E.R. Kenawy, F.I. Abdel-Hay, M.H. El-Newehy, G.E. Wnek, Controlled release of ketoprofen from electrospun poly(vinyl alcohol) nanofibers, *Mater. Sci. Eng. , A* 459 (2007) 390-396.
- [51] D.G. Yu, X.Y. Li, X. Wang, J.H. Yang, S.W.A. Bligh, G.R. Williams, Nanofibers Fabricated Using Triaxial Electrospinning as Zero Order Drug Delivery Systems, *ACS Appl. Mater. Interfaces* 7 (2015) 18891-18897.
- [52] S.F. Chou, D. Carson, K.A. Woodrow, Current Strategies for Sustaining Drug Release from Electrospun Nanofibers, *J. Controlled Release* 220 (2015) 584-591.
- [53] M. Eltayeb, E. Stride, M. Edirisinghe, Preparation, characterization and release kinetics of ethylcellulose nanoparticles encapsulating ethylvanillin as a model functional component, *J. Funct. Foods* 14 (2015) 726-735.
- [54] M. Eltayeb, E. Stride, M. Edirisinghe, A. Harker, Electrospayed nanoparticle delivery system for controlled release, *Mater. Sci. Eng., C* 66 (2016) 138-146.

Figure and Table Captions

Table Caption

Table 1. Parameters of ES process.

Table 2. Model parameters for GLSP release from ZP fibers. R^2 and n represent correlation coefficient and release exponent, respectively. k_H , k_{HC} and k demonstrate the release rate in each analysis.

Figures Captions

Figure 1. (a) Schematic diagram of the coaxial electrospinning (ES) set-up; (b) (I-III) dripping, spinning, and blocked modes during single-needle ES process; (c) (I-III) dripping, transition, and continuous spinning modes during coaxial ES process.

Figure 2. Scanning electron micrographs of electrospun ZP fibers obtained at various conditions: (a) single-needle electrospun fiber; (b) ZP-20; (c) ZP-40; (d) ZP-60; (e) ZP-80; (f) ZP-100; (g) schematic illustration of the cross sections of different ZP fibers.

Figure 3. Physical properties (viscosity and conductivity) of ethanol-water solutions.

Figure 4. Water contact angles on various fibrous membranes samples.

Figure 5. Effect of process parameters on mean fiber diameter using single-needle and coaxial ES operations: (a) flow rate (experimental conditions: flow rate of the outer Et.OH=1.0 mL/h, applied voltage=15.0 kV, and collector distance=15 cm); (b) applied voltage (experimental conditions: flow rate of both of the inner ZP solution and the outer Et.OH=1.0 mL/h, and collector distance=15 cm).

Figure 6. FTIR spectra of materials and samples prepared in this study.

Figure 7. (a) Effect of fiber morphology on GLSP encapsulation. (b) GLSP release profiles from ZP fibers prepared at different conditions.

Figure 8. (a) Cell viability evaluation of various composite fibrous membranes using

CCK-8 assay over a 24 hour test period. The viability of the control groups were set to 100%. (*P<0.05; N.S. means no significant difference); (b) Fluorescent images of L929 cells on various fibrous ZP membranes, presenting the cytocompatibility of different membranes with cells stained with phalloidin for cytoskeleton in red, DAPI for nuclei in blue, and merged images.

Tables

Table 1

Sample	Outer ethanol concentration (v/v%)	GLSP concentration (w/v%)	Outer flow rate (mL/h)	Inner flow rate (mL/h)	Voltage (kV)
ZP	-	-	-	1	15
ZP-20	20	-	1	1	15
ZP-40	40	-	1	1	15
ZP-60	60	-	1	1	15
ZP-80	80	-	1	1	15
ZP-100	100	-	1	1	15
ZP/GLSP	-	10	-	1	15
ZP-80/GLSP	80	10	1	1	15

Table 2

Samples	Higuchi model		Hixson-Crowell model		Korsmeyer-Peppas model		
	R ²	k _H	R ²	k _{HC}	R ²	k	n
ZP/GLSP	0.9366	3.09	0.9392	0.05	0.9004	66.56	0.26
ZP-40/GLSP	0.9944	1.45	0.9753	0.06	0.9850	62.98	0.20
ZP-60/GLSP	0.9728	2.03	0.9575	0.03	0.9410	49.77	0.26
ZP-80/GLSP	0.9728	2.52	0.9656	0.05	0.9410	61.94	0.26

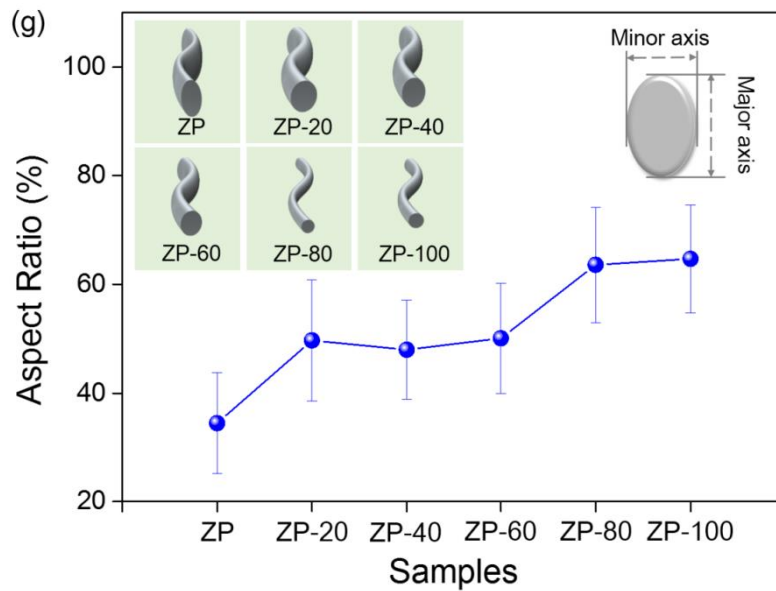
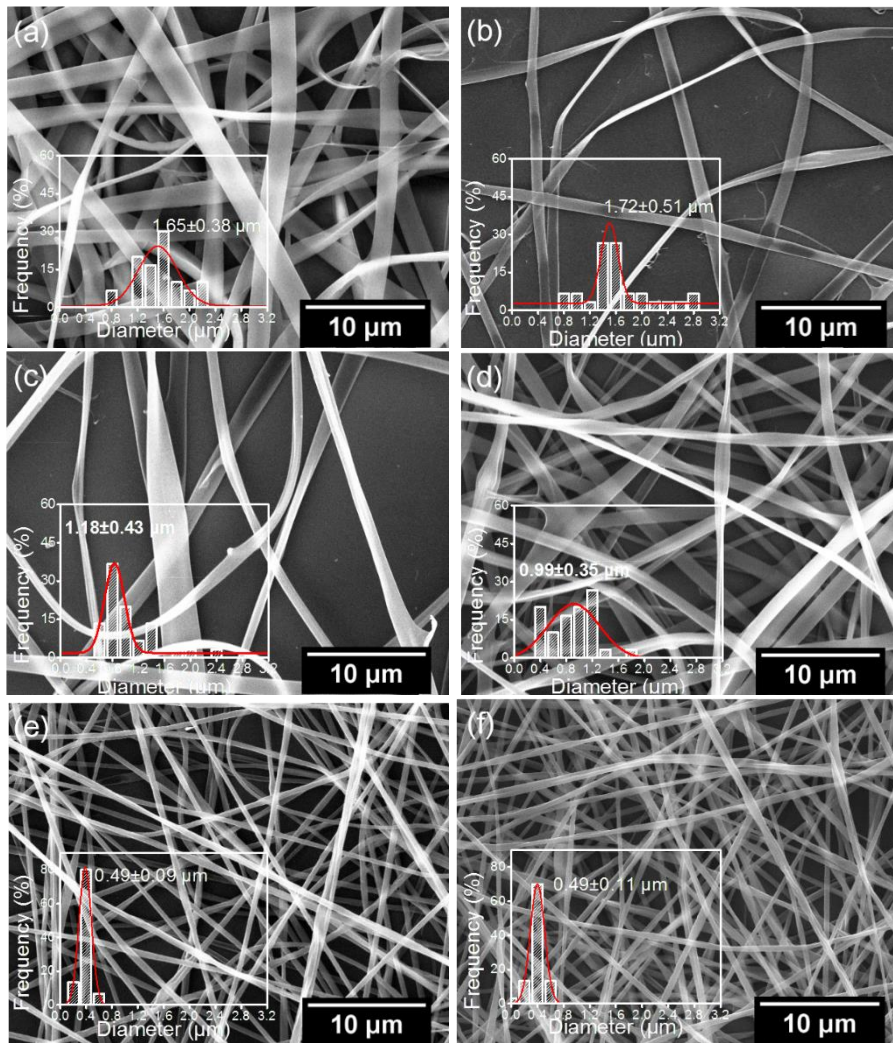


Figure 2

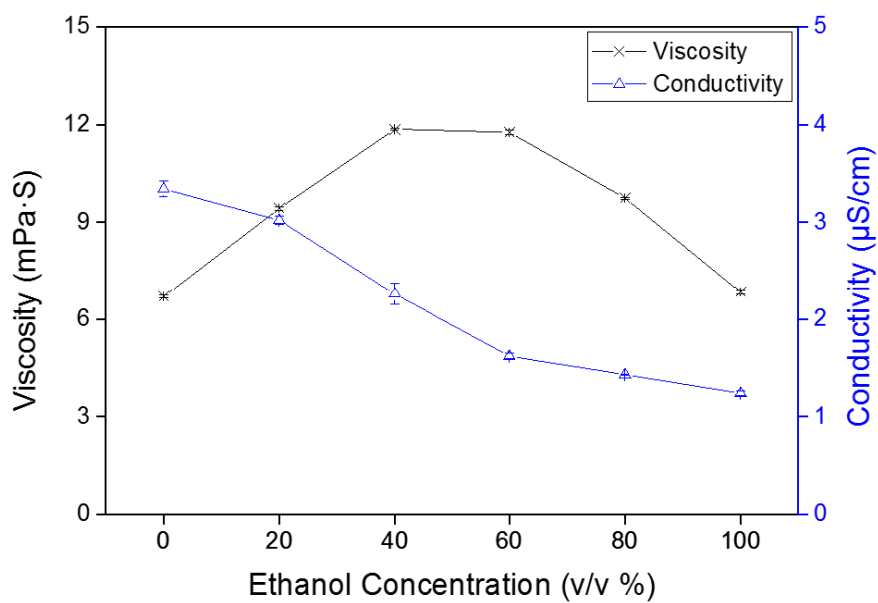


Figure 3

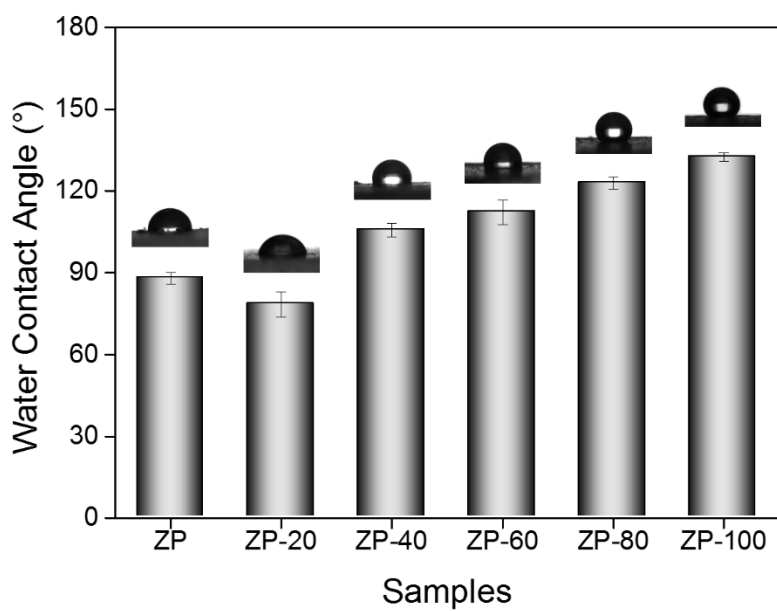


Figure 4

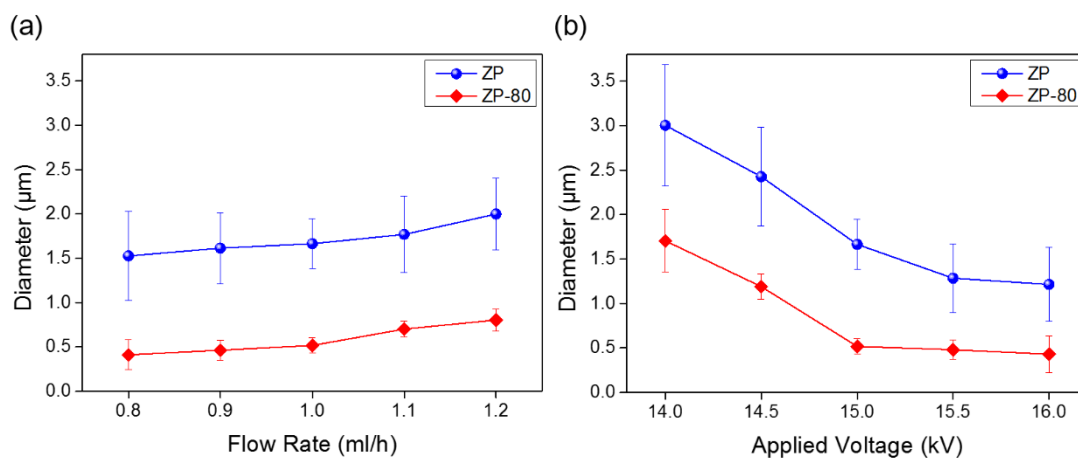


Figure 5

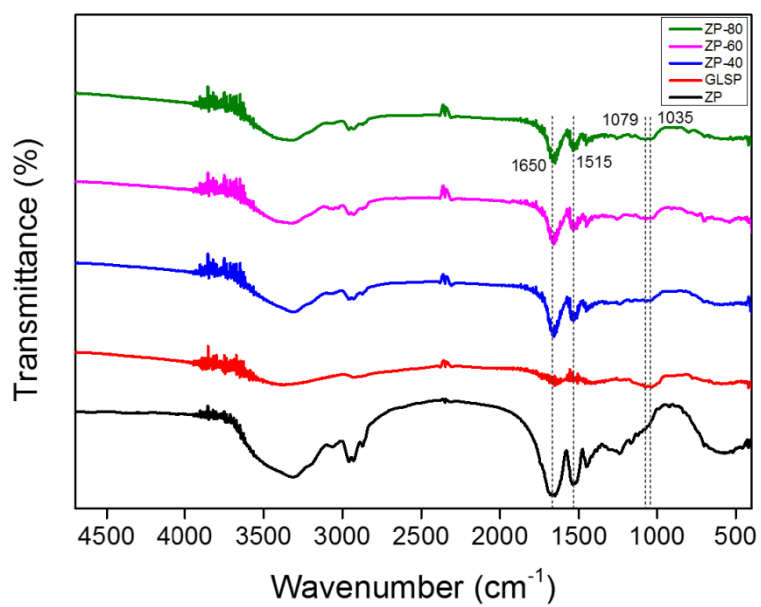


Figure 6

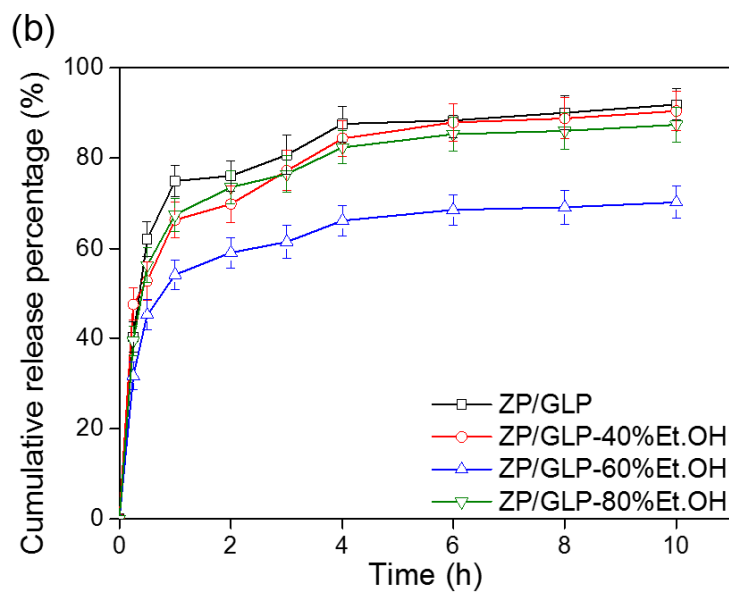
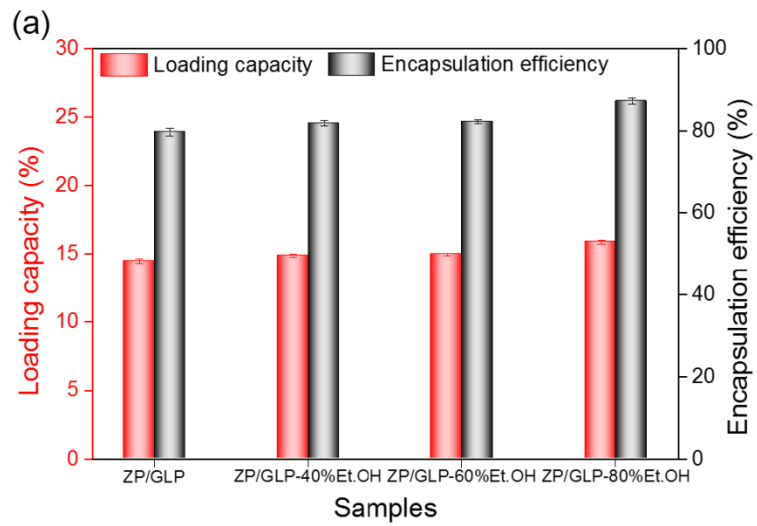


Figure 7

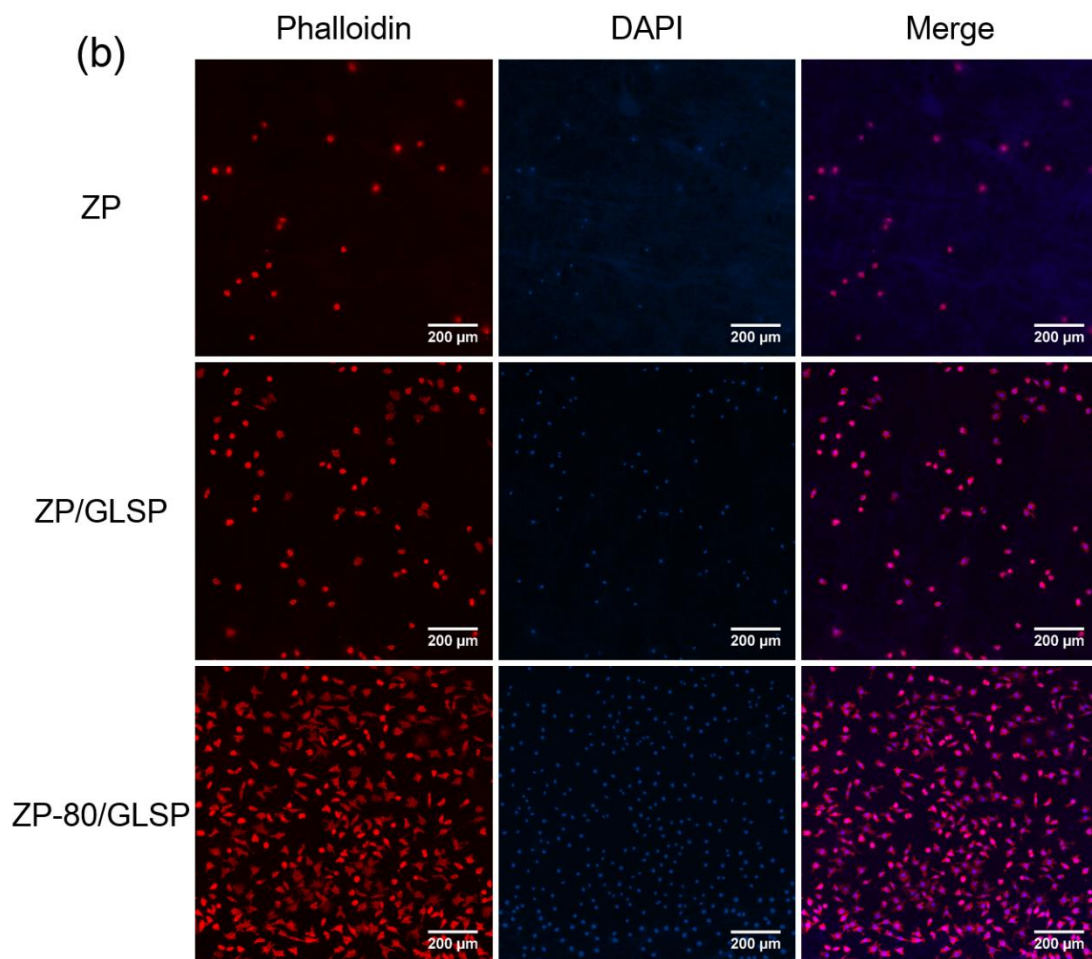
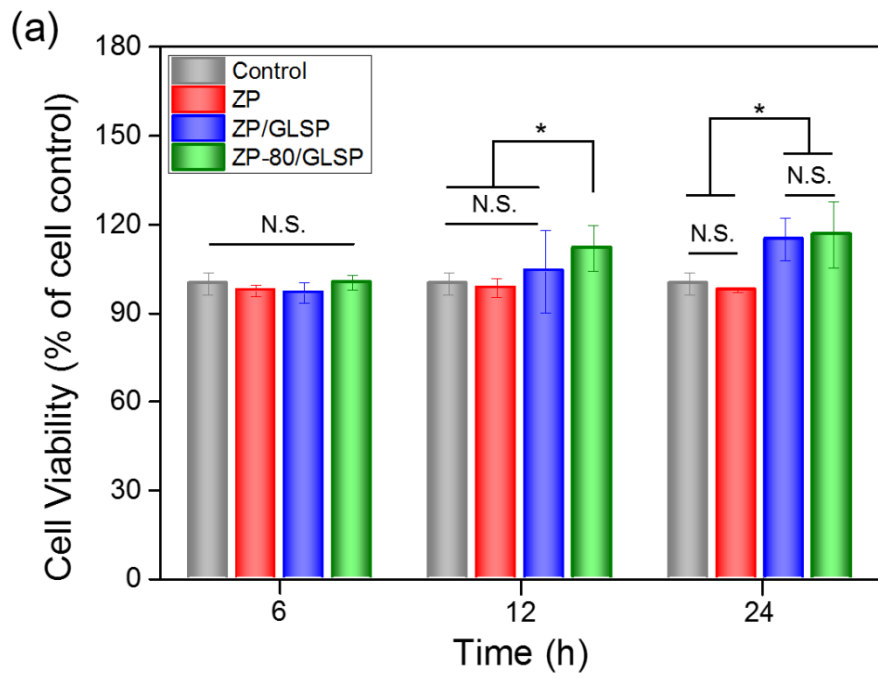


Figure 8